Commun. Comput. Phys.
doi: 10.4208/cicp.160609.311209a

Vol. **8**, No. 3, pp. 623-641
September 2010

Kernel Density Estimation Based Multiphase Fuzzy Region Competition Method for Texture Image Segmentation

Fang Li[1] and Michael K. Ng[2,*]

[1] *Department of Mathematics, East China Normal University, Shanghai 200241, China.*
[2] *Centre for Mathematical Imaging and Vision and Department of Mathematics, Hong Kong Baptist University, Kowloon Tong, Hong Kong.*

Received 16 June 2009; Accepted (in revised version) 31 December 2009

Available online 15 April 2010

Abstract. In this paper, we propose a multiphase fuzzy region competition model for texture image segmentation. In the functional, each region is represented by a fuzzy membership function and a probability density function that is estimated by a non-parametric kernel density estimation. The overall algorithm is very efficient as both the fuzzy membership function and the probability density function can be implemented easily. We apply the proposed method to synthetic and natural texture images, and synthetic aperture radar images. Our experimental results have shown that the proposed method is competitive with the other state-of-the-art segmentation methods.

AMS subject classifications: 62G86, 68U10, 94A08

Key words: Texture, multiphase region competition, kernel density estimation, fuzzy membership function, total variation.

1 Introduction

Image segmentation is a fundamental task in image processing and computer vision. It is aimed to partition an image into a finite number of subregions with homogeneous intensity (color, texture) properties which will hopefully correspond to objects or object parts. Approaches based on the calculus of variation and partial differential equations (PDEs) are powerful in image segmentation. One important reason of their success is that these models are flexible in integrating the geometric information such as shape, length and area. The best known and most influential approaches are Mumford-Shah

*Corresponding author. *Email addresses:* fli@math.ecnu.edu.cn (F. Li), mng@math.hkbu.edu.hk (M. K. Ng)

model [20], geodesic active contour [5], geodesic active region [23], Chan-Vese model [7], region competition [31].

In this paper, we focus on the segmentation of texture images. Piecewise smooth/constant models such as Mumford-Shah model [20] and Chan-Vese model [7] fail in this case. Recently, some variational methods have been proposed to tackle the segmentation of complex textures based on feature extraction techniques [9,14,25,27]. In [9,27], a set of Gabor filters with different scales, orientations and frequencies are applied to the image to create the features to represent texture in the image. Chan et al. in [9] extended the Chan-Vese model to these vector features for texture image segmentation. Because there are many features to be used in the model, the corresponding minimization method can be slow. Savig et al. [27] used the Beltrami framework on the texture features to define a new texture indicator function, and then integrated this function in a combined model of the geodesic active contour [5] and the vectorial Chan-Vese model [7] to segment textural regions. Rousson et al. [25] extracted the texture features by applying an anisotropic diffusion process to the structure tensor. In their segmentation framework, a Gaussian approximation is used for all the features channels, and a nonparametric approximation is used for the first gray image channel. The choice of Gaussian approximation restricts the applicability to limited set of images that satisfy the underlying assumption.

Another kind of variational methods for texture image segmentation is based on region competition. Zhu et al. [31] proposed a region competition method unifying snake, region growing and Bayesian statistics. It is a parametric model since they assume that each region follows a Gaussian distribution. Kim et al. in [16] proposed a nonparametric statistical method for image segmentation using mutual information and curve evolution. However, the above mentioned variational approaches have some practical shortcomings. The above energy functionals are not convex in the optimization space (usually the characteristic functions of sets, which is nonconvex collection) and they have local minima. Typically, the gradient decent method is used in the implementation of these models, and are therefore prone to getting stuck in these local minima. Hence these methods are sensitive to initialization. Meanwhile, the implementation of the above models are based on curve evolution and level set approach [22]. The drawback in the level set implementation consists of initializing the active contour in a distance function and re-initializing periodically during the evolution, which is time-consuming.

Based on the observation in the Rudin-Osher-Fatemi [26] model for binary image denoising and Chan-Vese segmentation model, the drawback of leading to local minima comes from the non-convexity of characteristic functions. Recently, Chan et al. [10] proposed to use a "segmentation" variable valued in $[0,1]$ to substitute a characteristic function and obtain a new constrained convex functional such that the global minimizer can be achieved in the segmentation process. To make the algorithm more efficient, Bresson et al. [2] proposed to add another new variable to approximate "segmentation" variable such that the Chambolle's fast dual projection method [6] can be employed. The advantage of this algorithm is that it is fast and easy to implement. There are several works following this idea [3,4,14,18,19]. Mory et al. [18,19] derived the fuzzy region competi-

tion method, parametric and nonparametric statistics error functions in the region terms are considered and studied respectively. Ni et al. [4] used histogram and Wasserstein distance in the region term. Houhou et al. [14] used shape operator borrowed from different geometry to extract only one texture feature and then used the popular Kullback-Leiber distance in the region term. We remark that the above techniques are only used in two-phase image segmentation.

In [28], Shen developed a multiphase stochastic variational soft segmentation Mumford-Shah model employed a double well potential regularization term in the model. As a set of partial differential equations arising from the model have to be solved, the resulting method is computationally expensive. This method may not be handled a more complicated texture image segmentation problem.

In this paper, we propose a multiphase fuzzy region competition model for texture image segmentation. In the functional, each region is represented by a fuzzy membership function and a probability density function. The fuzzy membership function is used to represent the region such that the energy functional is convex with respect to membership functions. The probability density function is estimated in each region by using kernel density method. The estimation method is different from [16, 19]. The overall algorithm is very efficient as both the fuzzy membership function and the probability density function can be implemented easily. We apply the proposed method to synthetic and natural texture images, and synthetic aperture radar images. Our experimental results have shown that the proposed method is competitive with the other state-of-the-art segmentation methods.

The outline of the paper is as follows. We review some related work for texture image segmentation in Section 2. In Section 3, we propose our method and the numerical algorithm. Experimental results on various images are showed in Section 4. Finally, we conclude our paper in Section 5.

2 Related works

The general N-phase segmentation problem can be formulated as follows: Given an image $I:\Omega\to\mathbb{R}$, where the image domain Ω is a bounded and open subset of $\mathbb{R}^2$, the aim is to partition Ω into N regions $\{\Omega_i\}_{i=1}^N$, such that $\Omega_i\cap\Omega_j=\emptyset, j\neq i$, and $\bigcup_{i=1}^N\Omega_i=\Omega$ by certain suitable measure. We review some texture image segmentation methods which are closely related to our method.

2.1 Region competition

Zhu and Yuille [31] proposed to minimize the following energy

$$F(\Gamma,\{\alpha_i\})=\sum_{i=1}^{N}\Big\{\frac{\mu}{2}\int_{\partial\Omega_i}ds-\int_{\Omega_i}\log P_i(I|\alpha_i)dx\Big\}. \tag{2.1}$$

The first term within the braces is the length of the boundary curve $\partial\Omega_i$ for region Ω_i. $\Gamma=\bigcup_{i=1}^{N}\partial\Omega_i$ is the segmentation boundaries of the entire image. The second term is the sum of the cost for coding the intensity I into region Ω_i by the conditional probability distributions $-\log P_i(I|\alpha_i)$, where α_i is the parameter in the probability density function P_i. Usually a Gaussian probability density function is considered

$$P_i(I|\alpha_i)=\frac{1}{\sqrt{2\pi}\sigma_i}\exp\Big(-\frac{(I-\mu_i)^2}{2\sigma_i^2}\Big),$$

where $\alpha_i=(\mu_i,\sigma_i)$ are scalar parameters. Curve evolution technique is used in the implementation to solve the optimization problem in (2.1).

2.2 Two phase fuzzy region competition

In order to solve a general two-phase region competition problem as minimizing

$$F(\Gamma,\alpha_1,\alpha_2)=\int_{\partial\Omega_1}ds+\lambda\int_{\Omega_1}r_1^{\alpha_1}dx+\lambda\int_{\Omega_2}r_2^{\alpha_2}dx,$$

where the image region Ω is partitioned into Ω_1 and Ω_2, α_i is the region parameter of the region Ω_i, and $r_i^{\alpha_i}$ is error function, Mory et al. [18] proposed to use fuzzy membership function $u\in BV_{[0,1]}(\Omega)$ to represent the region and minimize the two-phase fuzzy region competition energy instead

$$F(u,\alpha_1,\alpha_2)=\int_{\Omega}|\nabla u|dx+\lambda\int_{\Omega}ur_1^{\alpha_1}dx+\lambda\int_{\Omega}(1-u)r_2^{\alpha_2}dx. \tag{2.2}$$

The fast dual projection method proposed by Chambolle [6] is introduced to solve the problem. The error functions in Chan-Vese model [7] $\big(r_i^{\alpha_i}=(I-c_i)^2\big)$, and the local version are studied in the paper.

In the later work [19], Mory et al. considered nonparametric probability density function as an error function and minimize

$$\begin{aligned}F(u,p_1,p_2)=&\int_{\Omega}|\nabla u|dx+\lambda\int_{\Omega}u\int_{a\in\mathscr{A}}\Big(p_1(a)-K\big(I(x)-a\big)\Big)^2dadx\\&+\lambda\int_{\Omega}(1-u)\int_{a\in\mathscr{A}}\Big(p_2(a)-K\big(I(x)-a\big)\Big)^2dadx,\end{aligned} \tag{2.3}$$

where K is a symmetric Gaussian kernel

$$K(z)=\frac{1}{\sqrt{2\pi}\sigma}\exp\Big(-\frac{z^2}{2\sigma^2}\Big), \tag{2.4}$$

and $\mathscr{A}\subset\mathbb{R}$ is the values domain of the image. However, the computation is expensive since it involves the integration in domain $\mathscr{A}$.

2.3 Nonparametric method using mutual information

For two-phase image segmentation, Kim et al. [16] proposed to minimize the following energy

$$F(\vec{C}) = \alpha \int_{\vec{C}} ds - \frac{|\Omega|}{|\Omega_1|} \int_{\Omega_1} \log\Big(P_1\big(I(x)\big)\Big) dx - \frac{|\Omega|}{|\Omega_2|} \int_{\Omega_2} \log\Big(P_2\big(I(x)\big)\Big) dx, \tag{2.5}$$

where $\vec{C}$ is the curve of boundary $\partial\Omega_1$,

$$P_1\big(I(x)\big) = \frac{1}{|\Omega_1|} \int_{\Omega_1} K\big(I(x) - I(\hat{x})\big) d\hat{x}, \qquad P_2\big(I(x)\big) = \frac{1}{|\Omega_2|} \int_{\Omega_2} K\big(I(x) - I(\hat{x})\big) d\hat{x},$$

and K is a Gaussian kernel as defined in (2.4). The last two terms in the right hand side come from the mutual information. The derived curve evolution equation is

$$\begin{aligned} \frac{\partial \vec{C}}{\partial t} = \Bigg[& \log \frac{P_1\big(I(\vec{C})\big)}{P_2\big(I(\vec{C})\big)} + \frac{1}{|\Omega_1|} \int_{\Omega_1} \frac{K\big(I(x) - I(\vec{C})\big)}{P_1\big(I(x)\big)} dx \\ & - \frac{1}{|\Omega_2|} \int_{\Omega_2} \frac{K\big(I(x) - I(\vec{C})\big)}{P_2\big(I(x)\big)} dx \Bigg] \vec{N} - \alpha\kappa\vec{N}, \end{aligned} \tag{2.6}$$

where κ is the curvature of the curve $\vec{C}$ and $\vec{N}$ is the unit outward normal of $\vec{C}$. The computation is quite complicated, especially for multiphase image segmentation.

3 The proposed method

3.1 The proposed energy

We propose to use nonparametric probability density function in the region competition model which energy is

$$E(\Gamma) = \sum_{i=1}^{N} \frac{\mu}{2} \int_{\partial\Omega_i} ds - \sum_{i=1}^{N} \int_{\Omega_i} \log P_i(I, \Omega_i) dx. \tag{3.1}$$

Here $P_i(I, \Omega_i)$ is the nonparametric probability density function which is determined by the intensity values of pixels in region Ω_i. In the case of $N = 2$, the proposed energy is similar to (2.5). However, the numerical techniques are quite different. In the following, we will derive a quite simple and effective numerical method for the proposed model.

With a suitable change of the variables and parameters, (3.1) becomes

$$E(\chi) = \sum_{i=1}^{N} \int_{\Omega} |\nabla \chi_i| dx - \sum_{i=1}^{N} \lambda \int_{\Omega} \chi_i \log P_i(I, \chi_i) dx, \tag{3.2}$$

where $\chi=(\chi_1,\cdots,\chi_N)$ and χ_i is the characteristic function of the region Ω_i. The energy (3.2) is non-convex since the set of characteristic functions are not convex. To overcome this drawback, following the idea of [18], we replace the characteristic functions χ_i by fuzzy membership functions $u_i\in BV_{[0,1]}(\Omega)$. Note that $BV_{[0,1]}(\Omega)$ is the set of bounded variation functions valued in the interval $[0,1]$. Hence our new fuzzy region competition image segmentation model is to minimize the following energy

$$E(U,P)=\sum_{i=1}^{N}\int_{\Omega}|\nabla u_i|dx-\sum_{i=1}^{N}\lambda\int_{\Omega}u_i\log P_i(I,u_i)dx, \tag{3.3}$$

where the membership functions $\{u_i\}$ satisfies two constraints

$$\text{(i)}\quad u_i\in BV_{[0,1]}(\Omega),\quad\text{and}\quad\text{(ii)}\quad\sum_{i=1}^{N}u_i=1,$$

and $U=(u_1,\cdots,u_N)$, $P=(P_1,\cdots,P_N)$. Note that the term $\int_{\Omega}|\nabla u_i|dx$ is a total variation regularization term which is widely used in variational image processing.

For the purpose of efficiency in numerical method, we follow the idea in [2,15,18,19] and take use of Chambolle's fast dual projection algorithm [6]. For that end we add auxiliary variables $V=(v_1,\cdots,v_N)$, and approximate $E(U,P)$ by

$$\bar{E}(U,V,P)=\sum_{i=1}^{N}\Big(\int_{\Omega}|\nabla v_i|dx+\frac{1}{2\theta}\int_{\Omega}(v_i-u_i)^2dx-\lambda\int_{\Omega}u_i\log P_i(I,u_i)dx\Big), \tag{3.4}$$

where θ is chosen small enough such that u_i and v_i are almost identical with respect to the L^2 norm.

To make the constrained problem more easy to handle, we relax constraint (ii) by letting

$$u_N=1-\sum_{i=1}^{N-1}u_i, \tag{3.5}$$

and then further approximate the energy (3.4) by

$$\begin{aligned}E_r(U,\bar{V},P)=&\sum_{i=1}^{N-1}\int_{\Omega}|\nabla v_i|dx+\frac{1}{2\theta}\sum_{i=1}^{N-1}\int_{\Omega}(v_i-u_i)^2dx\\&+\lambda\sum_{i=1}^{N-1}\int_{\Omega}u_i\log\Big(\frac{P_N(I,u_N)}{P_i(I,u_i)}\Big)dx,\end{aligned} \tag{3.6}$$

subject to

$$0\le u_i(x)\le 1,\quad\text{for } i=1:N-1, \tag{3.7}$$

where $\bar{V}=(v_1,\cdots,v_{N-1})$.

3.2 Energy minimization

To find the minimizer of energy E_r in (3.6) under the constraint (3.7), we use an alternate minimization method.

3.2.1 Solving U

For fixed P and $\bar{V}$, we solve $\bar{U}=(u_1,\cdots,u_{N-1})$ by minimizing

$$E_1(\bar{U})=\frac{1}{2\theta}\sum_{i=1}^{N-1}\int_\Omega (v_i-u_i)^2dx+\lambda\sum_{i=1}^{N-1}\int_\Omega u_i\log\Big(\frac{P_N}{P_i}\Big)dx, \tag{3.8}$$

subject to

$$0\le u_i(x)\le 1,\quad \text{for } i=1:N-1.$$

Since the objective function is strictly convex and the feasible region is convex, there exists a unique global minimizer $\bar{U}^*=(u_1^*,\cdots,u_{N-1}^*)$ of (3.8) and the following KKT conditions [17] are both necessary and sufficient: Suppose $\tilde{U}^*$ is the global minimizer of (3.8), then

(a) $u_i^*(x)\ge 0$, $1-u_i^*(x)\ge 0$;

(b) There exist Lagrange multipliers $\beta_i^*(x)$ and $\gamma_i^*(x)$, for each point $x\in\Omega$, such that

$$\frac{\partial E_1(\bar{U})}{\partial u_i^*(x)}=\lambda\log\Big(\frac{P_N(x)}{P_i(x)}\Big)+\frac{1}{\theta}\Big(u_i^*(x)-v_i(x)\Big)=\beta_i^*(x)-\gamma_i^*(x);$$

(c) $\beta_i^*(x)u_i^*(x)=0$, $\gamma_i^*(x)\big(1-u_i^*(x)\big)=0$;

(d) $\beta_i^*(x)\ge 0$, $\gamma_i^*(x)\ge 0$;

for $i=1:N-1$.

First we assume $\tilde{U}=(\tilde{u}_1,\cdots,\tilde{u}_{N-1})$ satisfies

$$\lambda\log\Big(\frac{P_N(x)}{P_i(x)}\Big)+\frac{1}{\theta}\Big(\tilde{u}_i(x)-v_i(x)\Big)=0.$$

The solution is

$$\tilde{u}_i=v_i-\lambda\theta\log\Big(\frac{P_N}{P_i}\Big).$$

Then we construct $\hat{u}_i$ by projecting $\tilde{u}_i$ on $[0,1]$, that is $\hat{u}_i:=\min\big\{\max\{\tilde{u}_i,0\},1\big\}$. Let

$$\eta_i(x)=\lambda\log\Big(\frac{P_N(x)}{P_i(x)}\Big)+\frac{1}{\theta}\big(\hat{u}_i(x)-v_i(x)\big).$$

For each $x\in\Omega$, we choose $\hat{\beta}_i(x)$ and $\hat{\gamma}_i(x)$ as follows:

if $\hat{u}_i(x)\in(0,1)$, then we set $\hat{\beta}_i(x):=0$ and $\hat{\gamma}_i(x):=0$;

if $\hat{u}_i(x)=0$, then we set $\hat{\beta}_i(x):=\eta_i(x)\ge 0$ and $\hat{\gamma}_i(x):=0$;

if $\hat{u}_i(x)=1$, then we set $\hat{\beta}_i(x):=0$ and $\hat{\gamma}_i(x):=-\eta_i(x)\geq 0$.

It is easy to verify that $\{\hat{u}_i,\hat{\beta}_i,\hat{\gamma}_i\}$ satisfies KKT conditions (a)-(d). Therefore $\hat{U}$ is a minimizer of energy (3.8) and by uniqueness $\bar{U}^*=\hat{U}$.

Then we conclude that the closed form solution of u_i, $i=1:N-1$ is given by

$$u_i=\max\Big\{\min\Big\{v_i-\lambda\theta\log\Big(\frac{P_N}{P_i}\Big),1\Big\},0\Big\}, \tag{3.9}$$

and u_N is given by (3.5).

3.2.2 Estimation of P

Let us first give a brief introduction of nonparametric kernel density estimation method. If $y_1,y_2,\cdots,y_n\sim f$ is an independent and identically-distributed sample of a random variable, then the kernel density approximation of its probability density function (pdf) is

$$\hat{f}_h(y)=\frac{1}{nh}\sum_{j=1}^{n}K\Big(\frac{y-y_j}{h}\Big), \tag{3.10}$$

where K is some kernel and h is the bandwidth (smoothing parameter) [24]. In the proposed method K is taken to be a standard Gaussian kernel with mean zero and variance 1, i.e.,

$$K(z)=\frac{1}{\sqrt{2\pi}}\exp\Big(-\frac{z^2}{2}\Big). \tag{3.11}$$

We use the optimal bandwidth [1] for the Gaussian kernel density estimation, which is

$$h=(4/3n)^{\frac{1}{5}}\sigma,$$

where σ denotes the standard deviation of the distribution. A robust estimate of σ is the median absolute deviation estimator

$$\sigma=\text{median}\{|y_j-\mu|\}/0.6745,$$

where μ denotes the median of the sample. Remark that this pdf estimation is implemented by the function *ksdensity.m* in Matlab toolbox and we take use of it in our numerical implementation.

In our problem, for fixed U and $\bar{V}$, we need to estimate the probability density function $P_i(I,u_i)$ using the above method with Gaussian kernel. In the discrete form, assume the image I is a $p\times q$ matrix and $I(k,l),1\leq k\leq p,1\leq l\leq q$ denotes the intensity of the grid (k,l). Then we need to estimate the probability $P_i(k,l)$ at each grid. Now the question is how to choose y,y_j in (3.10), and how to assign the value of $P_i(k,l)$ from the estimated pdf $\hat{f}_h(y)$. In the simplest case of $N=2$, most of the intensity values can be classified into two categories: $I(k,l)\in R_i$, if $u_i(k,l)>0.5$. Then the intensity values in class R_i are regarded as

sample $\{y_j\}$. Since the range of the image is [0,255], we choose $y=[0:255]$ as the integers between 0 and 255. Hence we can estimate the pdf $\hat{f}_h(y)$ using formula (3.10). Finally, we assign $P_i(k,l)=\hat{f}_h\big(I(k,l)\big)$.

When the class number $N\geq 3$, P_i,i=1,$\cdots$,$N-1$ is estimated as the case of N=2. Remark that the Nth class is different from the other classes due to the relaxation (3.5) of the constraint (ii). Hence we use a non-uniform formula to estimate P_N in order to overcome the errors of chosen sample in the Nth class. We estimate P_N in the term $\log\big(P_N/P_i\big)$ by formula (3.10), where the sample is all the intensity values $I(k,l)$ satisfying $u_i(k,l)<0.5$.

3.2.3 Solving $\bar{V}$

By fixing P and U, the variables $\bar{V}$ can be solved by minimizing

$$\int_\Omega |\nabla v_i|dx+\frac{1}{2\theta}\int_\Omega (v_i-u_i)^2dx, \qquad i=1,\cdots,N-1. \tag{3.12}$$

This problem can be efficiently solved by fast duality projection algorithm. The solution is given by

$$v_i=u_i-\theta\text{div}\mathbf{p}_i, \tag{3.13}$$

where the vector $\mathbf{p}_i$ can be solved by fixed point method: initializing $\mathbf{p}_i^0=0$, and iterating

$$\mathbf{p}_i^{n+1}=\frac{\mathbf{p}_i^n+\tau\nabla\left(\text{div}\mathbf{p}_i^n-u_i/\theta\right)}{1+\tau\left|\nabla\left(\text{div}\mathbf{p}_i^n-u_i/\theta\right)\right|},$$

with $\tau\leq 1/8$ to ensure convergence. See [6] for more details. Furthermore, for this minimization problem, we can prove the existence and uniqueness of minimizer. We can also prove that the range of v_i is [0,1], if $u_i\in[0,1]$. It is the following proposition.

Proposition 3.1. There exists a unique minimizer v_* to minimization problem

$$\min_{v\in BV(\Omega)\cap L^2(\Omega)}\Big\{\int_\Omega |Dv|dx+\frac{1}{2\theta}\int_\Omega (v-u)^2dx\Big\}, \tag{3.14}$$

where $0\leq u\leq 1$. Moreover, v_* satisfies maximum principle

$$0\leq \operatorname*{essinf}_\Omega u\leq v_*\leq \operatorname*{esssup}_\Omega u\leq 1. \tag{3.15}$$

Remark that in the energy, we use $\int_\Omega |Dv|dx$ instead of $\int_\Omega|\nabla v|dx$, in order to indicate that the derivative is actually a measure. The proof of Proposition 3.1 can be found in the appendix.

3.3 The algorithm

The algorithm of minimizing E can be summarized in the following four steps:

1. Initialize the membership functions $u_i, i=1:N$, such that the constraints (i) and (ii) are both satisfied;
2. Estimate P_i by the method in Section 3.2.2;
3. Update v_i by formula (3.13) for $i=1:N-1$;
4. Update u_i by formula (3.9) for $i=1:N-1$ and (3.5) for $i=N$.

Repeat Steps 2-4 until termination. The termination criterion is as follows

$$\|U_{new}-U_{old}\|\leq\epsilon,$$

where $\|\cdot\|$ denotes the Euclidean distance, and ϵ is a small positive number.

4 Experimental results

We test our algorithm on various images include synthetic texture images, natural images and synthetic aperture radar (SAR) images which appear in the recent image segmentation literatures. We display the segmentation results by paint the contour $u_i=0.5$ $(i=1:N-1)$ with different colors on the original image. The membership functions are also displayed for illustration. Some of our results are compared with other state-of-the-art segmentation methods. In the numerical implementation, the fixed parameters are $\theta=0.1$, $\tau=0.125$. λ is a parameter that need to be tuned.

Test 1: Two-phase segmentation for synthetic texture images. Fig. 1 shows six synthetic texture images with the two-phase segmentation results by the proposed algorithm. The results are satisfactory. Parameters for the six images from left to right and up to bottom are $\lambda=0.3$, $\lambda=0.2$, $\lambda=0.2$, $\lambda=0.2$, $\lambda=0.1$, $\lambda=0.2$ in turn.

Test 2: Two-phase segmentation for synthetic images satisfying different distributions. We test synthetic images generated by several sets of distributions in Fig. 2 as used in [16]. In Fig. 2(a) the two distributions for the foreground and the background are Gaussian with different means and the same variance. In Fig. 2(d) the two distributions for the foreground and the background are Gaussian with the same mean and different variances. For these two cases, the method of Yezzi et al. [30] would require the selection of the appropriate statistic (i.e., the means and variances for the first and second cases, respectively) a priori, whereas our method solves the segmentation problem without a prior information. We see from Fig. 2 that the result is as well as that given in [16]. Fig. 2(g) shows a challenging case. The underlying distributions of the foreground and the background are a unimodal Gaussian density and a bimodal density with two Gaussian components as illustrated in Fig. 7(c)-(d) in [16]. The two distributions have the same mean and same variance, so it is hard even for a human observer to separate the

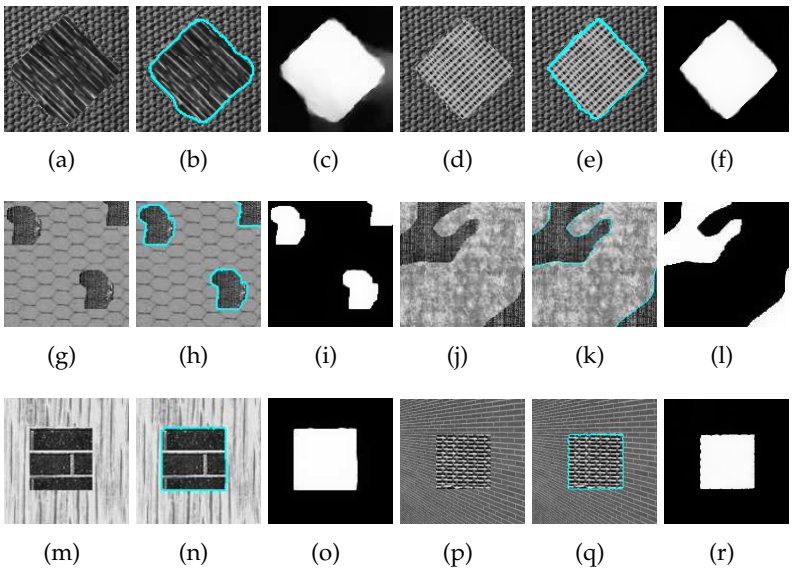

Figure 1: Two-phase segmentation for synthetic texture images. The First and Fourth columns: synthetic images; the Second and Fifth columns: segmentation results; the Third and Sixth columns: membership functions u_1. Parameters: $\lambda=0.3$ for (a); $\lambda=0.2$ for (d); $\lambda=0.2$ for (g); $\lambda=0.2$ for (j); $\lambda=0.1$ for (m); $\lambda=0.2$ for (p).

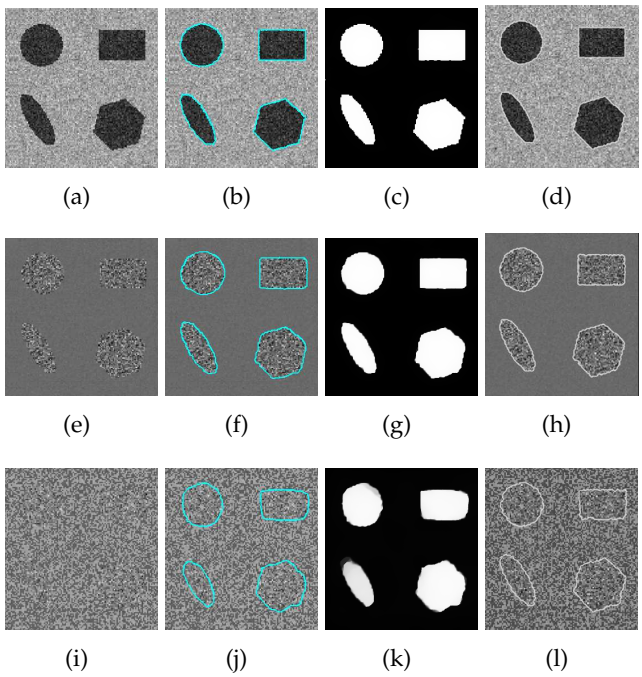

Figure 2: Two-phase segmentation for synthetic images satisfying different distributions. The First column: synthetic images; the Second column: segmentation results of the proposed method; the Third column: membership functions u_1 in the proposed method; the Fourth column: segmentation results by method in [16]. Parameters: $\lambda=0.2$ for (a); $\lambda=0.2$ for (e); $\lambda=0.5$ for (i).

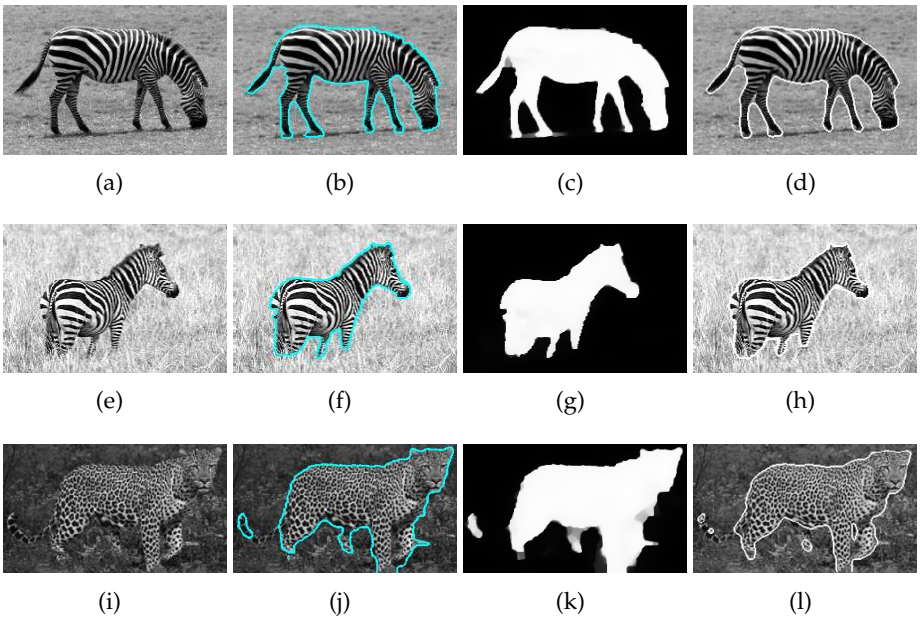

Figure 3: Two-phase segmentation for natural texture images. The First column: natural images; the Second column: segmentation results; the Third column: membership functions u_1; the Fourth column: segmentation results by method in [25]. Parameters: $\lambda=0.2$ for (a); $\lambda=0.3$ for (e); $\lambda=0.3$ for (i).

foreground from the background. However, our method still gives good segmentation results which are competitive with the results by method in [16]. Parameters for Fig. 2(a), Fig. 2(e) and Fig. 2(i) are $\lambda=0.2$, $\lambda=0.2$ and $\lambda=0.5$ respectively.

Test 3: Two-phase segmentation for natural texture images. In Fig. 3, three natural texture images are tested. Compared with the results of the state-of-the-art works showed in Fig. 3, our results are also satisfactory. Parameters for the proposed method for the three images are $\lambda=0.2$, $\lambda=0.3$ and $\lambda=0.3$ in turn.

Test 4: Three-phase image segmentation. In Fig. 4, we test our method with 3-phase image segmentation. The segmentation results are still satisfactory. Parameters for Fig. 4(a) and Fig. 4(e) are $\lambda=0.2$ and $\lambda=0.3$ respectively.

Test 5: Four-phase image segmentation. In Fig. 5, we test our method with 4-phase image segmentation. The segmentation results are satisfactory. The parameter is $\lambda=0.3$.

Test 6: Sensitivity to initialization (two-phase case). In Fig. 6, we illustrate the evolution of membership function with different initializations for the zebra image in Fig. 3(e). In Fig. 6(a) and Fig. 6(e), we initialize $u_1=1$ in the white circle, and otherwise $u_1=0$. In Fig. 6(i), we set the initial membership function $u_1=I/255$. In Fig. 6(m), we choose the initial membership function randomly valued in $[0,1]$. Fig. 6 shows that our method is not sensitive to initialization which is a drawback of active contour based method. However, the running time of the proposed method depends on the initialization. Good initial-

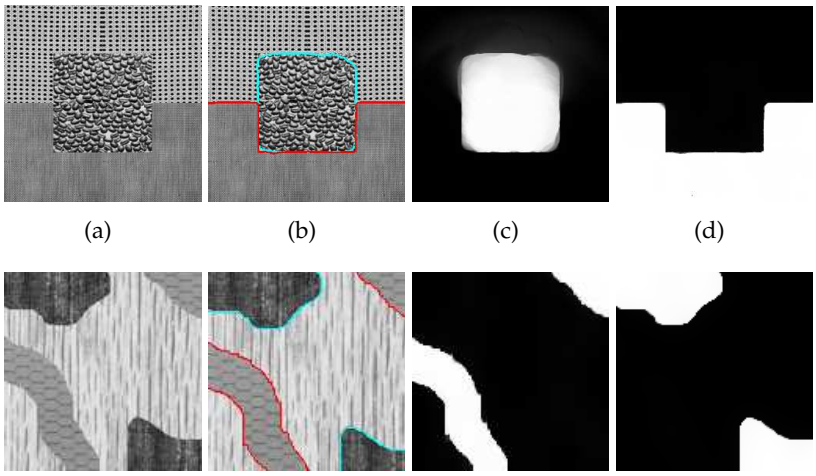

(a) (b) (c) (d)

(e) (f) (g) (h)

Figure 4: Three-phase image segmentation. The First column: synthetic images; the Second column: segmentation results; the Third column: membership functions u_1; the Fourth column: membership functions u_2. Parameters: $\lambda=0.2$ for (a), $\lambda=0.3$ for (e).

(a) (b) (c) (d) (e)

Figure 5: Four-phase image segmentation. (a) synthetic image; (b) segmentation result; (c) membership function u_1; (d) membership function u_2; (d) membership function u_3. Parameter: $\lambda=0.3$.

ization such as Fig. 6(a) converges faster than other initializations. We remark that by experience, the best initialization in terms of speed is obtained by choosing characteristic function of a region inside the object to be segmented. The parameter is $\lambda=0.3$.

Test 7: Sensitivity to initialization (three-phase case). Remark that for $N\geq 3$, the algorithm is also sensitive to initialization of membership functions. A good initialization of $u_i, i=1,\cdots,N-1$ is given by first choosing a part almost inside the i-th texture region and then initializing $u_i=1, u_j=0, j\neq i$ in that region. This initialization method is used to get the results for $N\geq 3$ in this paper if not specified. In Fig. 7, we show two initializations of Fig. 4(e). One gives the correct result (First row) and the other gives the wrong result (Second row). We can see from Fig. 7(g) and Fig. 7(h) that $u_1+u_2\approx 1$, $u_3\approx 0$, thus the image is finally segmentated into two regions but not three regions. The parameter is $\lambda=0.3$.

In the following, we make comparison with our method and the anisotropic heat diffusion based method in [12] for SAR image segmentation. SAR image segmentation is

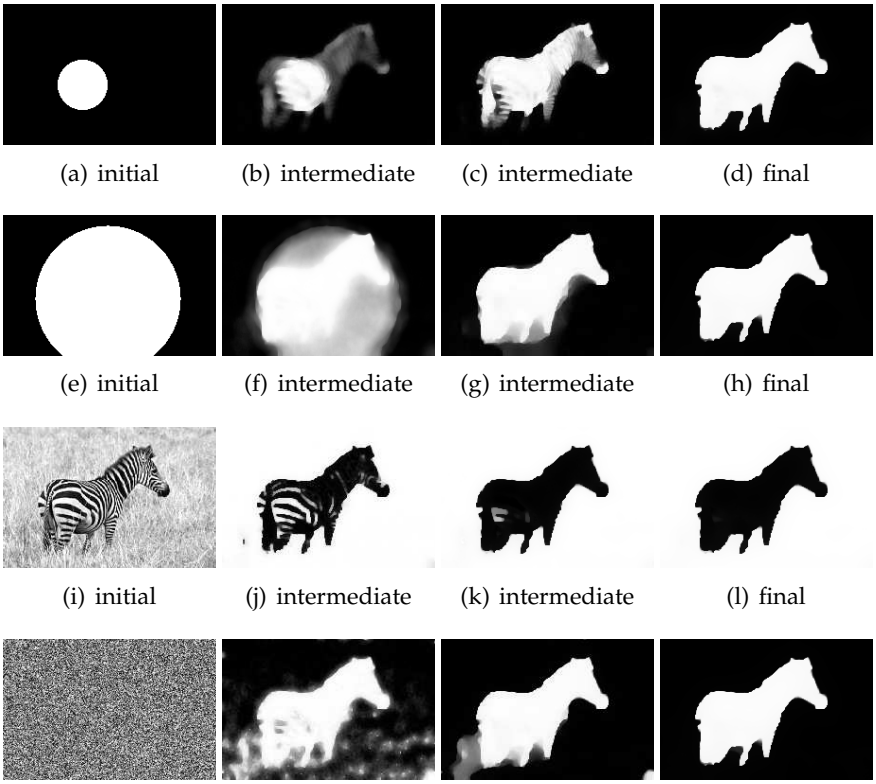

(a) initial (b) intermediate (c) intermediate (d) final

(e) initial (f) intermediate (g) intermediate (h) final

(i) initial (j) intermediate (k) intermediate (l) final

(m) initial (n) intermediate (o) intermediate (p) final

Figure 6: Sensitivity to initialization (two-phase case). The figure displays the evolution of the membership functions with different initializations on a zebra image Fig. 3(e). The final results from top to bottom are obtained at iterations 105, 270, 150 and 240 respectively. Parameter: $\lambda = 0.3$.

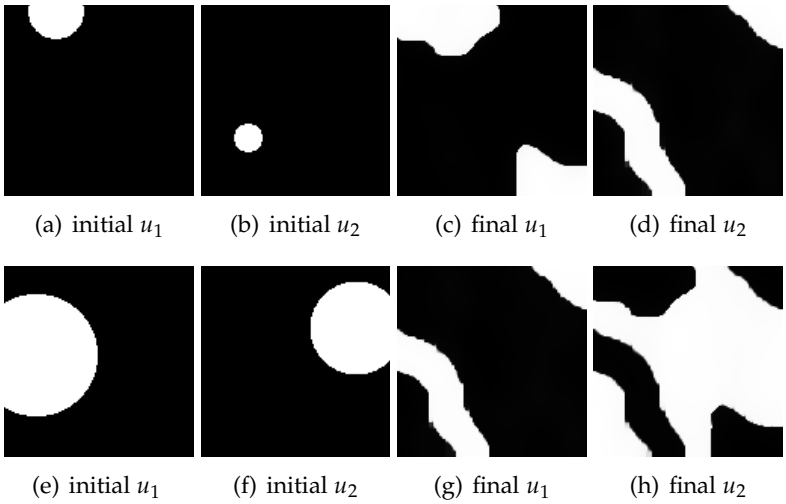

(a) initial u_1 (b) initial u_2 (c) final u_1 (d) final u_2

(e) initial u_1 (f) initial u_2 (g) final u_1 (h) final u_2

Figure 7: Sensitivity to initialization (three-phase case). The test image is Fig. 4(e). The First row: initialization 1 gives the correct result. Second row: initialization 2 gives the wrong result. Parameter: $\lambda = 0.3$.

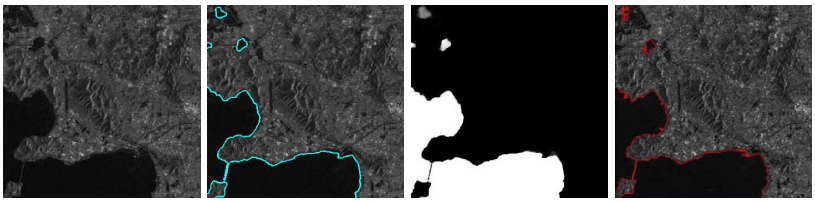

(a) (b) (c) (d)

Figure 8: Two-phase SAR image segmentation. (a) SAR images; (b) segmentation result by the proposed method; (c) membership functions u_1; (d) segmentation result by the method in [12]. Parameter: $\lambda = 0.08$.

(a) (b) (c) (d) (e)

Figure 9: Three-phase SAR image segmentation. (a) SAR image; (b) segmentation result by the proposed method; (c) membership function u_1; (d) membership function u_2; (e) segmentation result by method in [12]. Parameter: $\lambda = 0.2$.

usually said to be a complex problem in the pattern recognition area, due to the presence of speckle derived from the coherency of the image formation process. Since the pdf of the speckle noise follows some distribution, we can expect that the proposed segmentation model can segment this kind of image.

Test 8: Two-phase segmentation for a SAR image. Fig. 8(a) is a test SAR image contains Wujiang river in China which is tested in [12]. The water area is extracted in Fig. 8(d) by their method. Our method gives satisfactory segmentation results in Fig. 8(b) with a more accurate and smoother boundary. We take $\lambda = 0.08$ for this image.

Test 9: Three-phase segmentation for a SAR image. Fig. 9(a) shows a real MSTSAR SAR image of vehicle T72. This image mainly contains three regions: background, target and shadow. Fig. 9(b) shows the three-phase segmentation result of our proposed method. Fig. 9(c) and Fig. 9(d) display the membership functions u_1 and u_2. Our result is competitive with the result Fig. 9(e) by method in [12]. We take $\lambda = 0.2$ for this image.

5 Conclusions

A general multiphase fuzzy region competition model for texture image segmentation is proposed in this paper. There are two novelties. One is that a fuzzy membership function is introduced to represent a region for handling multiphase segmentation. The other is the use of kernel density estimation with optimal bandwidth to estimate the probabil-

ity density function in each region represented by the fuzzy membership function. The proposed method is faster and easier to implement than the other curve evolution based methods. According to our experimental results, we find that our method is competitive with other state-of-the-art segmentation methods for texture images and SAR images. In the future work, we will extend the proposed method to vector valued images.

Appendix

Proof of Proposition 3.1. Define φ and φ_ϵ on $\mathbb{R}^n$ by

$$\varphi(p)=|p|, \qquad \varphi_\epsilon(p)=\frac{1}{1+\epsilon}|p|^{1+\epsilon},$$

for $\epsilon>0$, and consider the following minimization problem

$$\min_{v\in W^{1,1+\epsilon}(\Omega)\cap L^2(\Omega)}\Big\{E_\epsilon(v)=\int_\Omega \varphi_\epsilon(\nabla v)dx+\frac{1}{2\theta}\int_\Omega (v-u)^2dx\Big\}.$$

It can be verified that $E_\epsilon(v)$ is lower semi-continuous since $W^{1,1+\epsilon}(\Omega)\cap L^2(\Omega)$ is a reflexive Banach space and $E_\epsilon(v)$ is strictly convex. By standard variational methods, there is a unique solution v_ϵ to this problem. We fix $\epsilon>0$, $t\geq 0$ and let $w=\min\{v_\epsilon,t\}$. Noting that

$$w\in W^{1,1+\epsilon}(\Omega)\cap L^2(\Omega),$$

with

$$\nabla w=\begin{cases}\nabla v_\epsilon, & \text{if } v_\epsilon<t,\\ 0, & \text{if } v_\epsilon\geq t,\end{cases}$$

we have

$$\int_\Omega \varphi_\epsilon(\nabla v_\epsilon)dx+\frac{1}{2\theta}\int_\Omega (v_\epsilon-u)^2dx\leq\int_\Omega \varphi_\epsilon(\nabla w)dx+\frac{1}{2\theta}\int_\Omega (w-u)^2dx, \tag{A.1}$$

and thus after subtracting

$$\int_{\{v_\epsilon\geq t\}} \varphi_\epsilon(\nabla v_\epsilon)dx+\frac{1}{2\theta}\int_{\{v_\epsilon\geq t\}} (v_\epsilon-u)^2dx\leq\frac{1}{2\theta}\int_{\{v_\epsilon\geq t\}} (t-u)^2dx.$$

Hence

$$\int_{\{v_\epsilon\geq t\}} (v_\epsilon-u)^2dx\leq\int_{\{v_\epsilon\geq t\}} (t-u)^2dx. \tag{A.2}$$

Setting $t=\operatorname{esssup}_\Omega u$, we see that if $\operatorname{esssup}_\Omega v_\epsilon>t$. Then

$$\int_{\{v_\epsilon\geq t\}} (t-u)^2dx<\int_{\{v_\epsilon\geq t\}} (v_\epsilon-u)^2dx,$$

which contradicts (A.2). Applying a similar argument to $w=\min\{v_\epsilon,t\}$, for $t=\text{essinf}_\Omega\ u$, we get $v_\epsilon \geq \text{essinf}_\Omega\ u$. Then

$$0\leq \operatorname*{essinf}_\Omega u\leq v_\epsilon \leq \operatorname*{esssup}_\Omega u\leq 1. \tag{A.3}$$

Furthermore, since (A.1) holds for any $w\in W^{1,1+\epsilon}(\Omega)\cap L^2(\Omega)$, letting $w=0$ in (A.1), we see that v_ϵ is bounded in $W^{1,1+\epsilon}(\Omega)\cap L^2(\Omega)\subset BV(\Omega)\cap L^2(\Omega)$ independent of ϵ. Thus there exists a $v_*\in BV(\Omega)\cap L^2(\Omega)$, and a subsequence of $\{v_\epsilon\}$, still denoted by $\{v_\epsilon\}$, such that $v_\epsilon\to v_*$ strongly in $L^1(\Omega)$, $v_\epsilon \rightharpoonup v_*$ weakly in $L^2(\Omega)$, and $v_\epsilon\to v_*$ a.e. in Ω. Letting $\epsilon\to 0$ in (A.1), noting that $\varphi(p)\leq\varphi_\epsilon(p)$, for all p,

$$\int_\Omega \varphi_\epsilon(\nabla w)\to\int_\Omega \varphi(\nabla w),$$

lower semicontinuity of the functional $\int_\Omega\varphi(p)dx$ on $BV(\Omega)$, and the lower semicontinuity of L^2 norm, we get

$$\int_\Omega \varphi(Dv_*)dx+\frac{1}{2\theta}\int_\Omega (v_*-u)^2dx\leq\int_\Omega\varphi(\nabla w)dx+\frac{1}{2\theta}\int_\Omega(w-u)^2dx, \tag{A.4}$$

for all $w\in W^{1,1+\epsilon}(\Omega)\cap L^2(\Omega)$. Note that for any $w\in BV(\Omega)\cap L^2(\Omega)$, there exists a sequence w_n in $C^\infty(\bar{\Omega})$, such that

$$\int_\Omega\varphi(\nabla w_n)dx\to\int_\Omega\varphi(Dw)dx,$$

and $w_n\to w$ strongly in $L^2(\Omega)$ [13]. Hence (A.4) holds for all $w\in BV(\Omega)\cap L^2(\Omega)$, and then v_* is a minimizer of problem (3.14). The uniqueness of minimizer follows by the strict convexity of the energy functional in (3.14). By inequality (A.3), v_* satisfies maximum principle (3.15). □

Acknowledgments

The authors would like to thank the two referees for their useful suggestions to the manuscript. The paper is supported partially by RGC 201508, HKBU FRGs, The Research Fund for the Doctoral Program of Higher Education (200802691037) and the Natural Science Foundation of Shanghai (10ZR1410200).

References

[1] A. W. Bowman and A. Azzalini, Applied Smoothing Techniques for Data Analysis, Oxford University Press, 1997.
[2] X. Bresson, S. Esedoglu, P. Vandergheynst, J.-P. Thiran and S. Osher, Fast global minimization of the active contour/snake model, J. Math. Imaging. Vis., 28 (2007), 151–167.
[3] X. Bresson and T.F. Chan, Non-local unsupervised variational image segmentation models, UCLA cam report 08-67.

[4] K. Ni, X. Bresson, T. F. Chan and S. Esedoglu, Local histogram based segmentation using the wasserstein distance, UCLA cam report cam 08-47.
[5] V. Caselles, R. Kimmel and G. Sapiro, Geodesic active contours, Int. J. Comput. Vis., 1 (1997), 61–79.
[6] A. Chambolle, An algorithm for total variation minimization and applications, J. Math. Imaging. Vis., 20 (2004), 89–97.
[7] T. F. Chan and L. A. Vese, Active contour without edges, IEEE. T. Image. Process., 10 (2001), 266–277.
[8] T. F. Chan and L. A. Vese, Active Contour and Segmentation Models Using Geometric PDE's for Medical Imaging, Malladi, R. (Ed.), Geometric Methods in Bio-Medical Image Processing, Series: Mathematics and Visualization, Springer, 2002.
[9] T. Chan, B. Sandberg and L. Vese. Active contours without edges for vector-valued images, J. Vis. Commun. Image. R., 11 (2000), 130–141.
[10] T. F. Chan, S. Esedoglu and M. Nikolova, Algorithms for finding global minimizers of image segmentation and denoising models, SIAM. J. Appl. Math., 66 (2006), 1632–1648.
[11] L. C. Evans and R. F. Gariepy, Measure Theory and Fine Properties of Functions, CRC Press, Boca Raton, FL, 1992.
[12] G. Gao, L. Zhao, J. Zhang, D. Zhou and J. Huang, A segmentation algorithm for SAR images based on the anisotropic heat diffusion equation, Pattern. Recogn., 41 (2008), 3035–3043.
[13] R. Hardt and D. Kinderlehrer, Elastic plastic deformation, Appl. Math. Optim., 10 (1983), 203–246.
[14] N. Houhou, J. P. Thiran and X. Bresson, Fast texture segmentation model based on the shape operator and active contour, Proc. Cvpr. IEEE., 2008.
[15] Y. Huang, M. Ng and Y. Wen, A fast total variation minimization method for image restoration, SIAM. J. Multiscale. Modeling. Simulation., 7 (2008), 774–795.
[16] J. Kim, J. Fisher, A. Yezzi, M. Cetin and A. Willsky, A nonparametric statistical method for image segmentation using information theory and curve evolution, IEEE. Trans. Image. Process., 14 (2005), 1486–1502.
[17] H. W. Kuhn and A. W. Tucker, Nonlinear Programming, Proceedings of 2nd Berkeley Symposium, Berkeley: University of California Press, 1951.
[18] B. Mory and R. Ardon, Fuzzy region competition: a convex two-phase segmentation framework, F. Sgallari, A. Murli, and N. Paragios (Eds.), SSVM 2007, LNCS 4485, pp. 214-226, 2007.
[19] B. Mory and R. Ardon, Variational segmentation using fuzzy region competition and local non-parametric probability desity functions, ICCV 2007, IEEE 11^{th} international conference on computer vision, pp. 1–8.
[20] D. Mumford and J. Shah, Optimal approximations by piecewise smooth functions and associated variational problems, Comm. Pure. Appl. Math., 42 (1989), 577–685.
[21] Mila Nikolova, Selim Esedoglu and Tony F. Chan, Algorithms for finding global minimizers of image segmentation and denoising models, SIAM. J. Appl. Math., 66 (2006), 1632–1648.
[22] S. Osher and N. Paragios, Geometric Level Set Methods in Imaging Vision and Graphics, Springer Verlag, 2003.
[23] N. Paragios and R. Deriche, Geodesic active regions: a new paradigm to deal with frame partition problems in computer vision, J. Vis. Commun. Image. R., 13 (2002), 249–268.
[24] E. Parzen, On the estimation of a probability density function and mode, Ann. Math. Stat., 33 (1962), 1065–1076.
[25] M. Rousson, T. Brox and R. Deriche, Active unsupervised texture segmentation on a dif-

fusion based feature space, In Proc. 2003 IEEE Computer Society Conference on Computer Vision and Pattern Recognition, CVPR03, June 2003.

[26] L.I. Rudin, S. Osher and E. Fatemi, Nonlinear total variation based noise removal algorithms, Physica. D., 60 (1992), 259–268.

[27] C. Sagiv, N. A. Sochen and Y. Y. Zeevi, Texture segmentation via a diffusion-segmentation scheme in the gabor feature space, In Proc. Texture 2002, 2nd International Workshop on Texture Analysis and Synthesis, Copenhagen, June 2002.

[28] J. Shen, A stochastic-variational model for soft Mumford-Shah segmentation, I. S. Biomed. Imaging., 2006, Article ID 92329, pp. 1-14.

[29] R.A. Weisenseel, W.C. Karl, D.A. Castanon and R.C. Brower, MRF-based algorithms for segmentation of SAR images, IEEE Proceeding of the 1998 International Conference on Image Processing, 3 (1998), 770–774.

[30] A. Yezzi, Jr., A. Tsai and A. Willsky, A statistical approach to snakes for bimodal and trimodal imagery, Int. J. Comput. Vision., 1999, 898–903.

[31] S. C. Zhu and A. Yuille, Region competition: unifying snakes, region growing, and bayes/mdl for multiband image segmentation, IEEE. T. Pattern. Anal., 18 (1996), 884–900.